Effects of small amount of active Ti element additions on microstructure and property of Sn3.5Ag0.5Cu solder

C.L. Chuang [a,b], L.C. Tsao [c,*], H.K. Lin [c], L.P. Feng [c]

[a] Department of Occupational Safety and Health, Chung Shan Medical University, No. 110, Sec. 1, Chien-Kuo N. Road, Taichung 402, Taiwan
[b] Department of Medical Research, ChungShan Medical University Hospital, No. 110, Sec. 1, Chien-Kuo N. Road, Taichung 402, Taiwan
[c] Graduate Institute of Materials Engineering, National Pingtung University of Science & Technology, 1, Seuhfu Road, Neipu, Pingtung 91201, Taiwan

ARTICLE INFO

ABSTRACT

The present work investigated the effect of adding a small amount of Ti on the microstructure, physical and mechanical properties of Sn3.5Ag0.5Cu (SAC) solder. The results indicated that adding a small amount of Ti can slightly decrease both the melting temperature and melting range of the SAC solder alloy and that it can also effectively refine the microstructure. The eutectic colony becomes rather narrower with the addition of Ti into SAC, and the microhardness, YS, and UTS are significantly higher than to those of the other commercially available SAC solder alloys. Microstructural analysis revealed that the origin of change in mechanical properties was due to refined β-Sn grains and the formation of new Ti_2Sn_3 inter-metallic compounds (IMC) in the SAC-XTi solder alloys. However, when the concentration of Ti exceeded 1.0 wt%, the benefits of elongation were reduced due to the small amount of coarse Ti_2Sn_3 in the eutectic colonies.

© 2012 Elsevier B.V. All rights reserved.

1. Introduction

Owing to considerations of environmental protection and human health, the adoption of lead-free solder has become an inevitable trend in the electronics industry. Among the various lead-free solder alloys, Sn–Ag–Cu (SAC) systems have been proposed as the most promising substitutes for tin–lead solder in reflow applications due to their relatively low melting temperature, generally superior mechanical properties, and relatively good solder abilities [1–3]. However, many issues with the SAC solders still remain unresolved, such as the best composition, the large undercooling in solidification, and the formation of large, brittle inter-metallic compounds (IMC) [4]. Especially, alloys with high Ag content exhibit the formation of large Ag_3Sn platelets at the solder-reaction layer interfaces, regardless of the kind of substrate [5]. However, in meeting the demand for the miniaturization of integrated circuits, novel lead-free solders with better performance and reliability from interconnection BGA joints is needed. In order to further enhance the properties of Sn–Ag–Cu solder alloys, alloying elements such as transition metals, rare earths and nanoparticles were selected by addition into these alloys [6–14]. For e.g., Pb-free solders doped with nano-sized, non-reacting, non-coarsening oxide dispersoids have been identified as potential materials that could provide higher microstructure stability and better mechanical properties than the conventional solders, such as in TiO_2 [7,8], A_2O_3 [9,10], SiC [11] and ZrO_2 [12]. Another, adding minute amount of rare earth (RE) to the solder alloy is considered to

be an effective way to improve the high temperature performance of solders [13,14]. RE elements are the surface-active element, which plays an important role in metallurgy of materials, such as refinement of microstructure, alloying and purification of materials and metamorphosis of inclusions. However, in the past decade, China has tightened control of rare earth exports by introducing export quotas that have been reduced each year, which is making the rare earth elements relatively expensive [15].

It is well known that Ti is highly chemically active. It has been widely used in the aluminum industry for the refining of cast microstructures, which can increase both the strength and ductility of alloys [16]. Another application is in the bonding of non-wettable materials, such as ceramics, glass, and graphite [17]. Liu et al. [18] and Liu and Lee [19] reported that doping with a small amount of Ti brings a pronounced improvement in drop test performance of SAC solder joints. In order to further enhance the properties of Sn3.5Ag0.5Cu (SAC) solder alloys, trace amounts of Ti have been used by researchers as alloying additions into Sn-based solders.

In this paper, we summarize the developments in SAC solder alloys with the addition of different amounts of Ti alloying elements, and their effects on the thermal analysis, microstructural and mechanical properties of SAC solder alloys.

2. Experimental procedures

2.1. Processing of lead-free solder

Sn3.5Ag0.5Cu(SAC), SAC–0.25Ti, SAC–0.5Ti, and SAC–1Ti solder alloys were fabricated in nominal weight percent compositions.

Pure tin (99.99%), silver (99.99%), copper (99.99%) and Ti (99.8%) were melted in a vacuum arc melting furnace to produce solder alloys of SAC–XTi solder ($X=0$–1.0 wt%), and they were subsequently remelted and cast into a water-cooled copper mold to form square ingots of $8 \times 10 \times 20$ mm³.

2.2. Differential scanning calorimetry

Differential scanning calorimetry (DSC, DSC6100, SEIKO) was used to determine the melting temperatures of the composite solders. The samples were examined under a nitrogen atmosphere on DSC with a sample of about 10 mg sealed in a hermetic aluminum pan. The kinetic curing profile was obtained by heating the formulated sample to a temperature of around 250 °C at a heating rate at 10 °C/min.

2.3. Microstructural characterization

The microstructure of the lead-free SAC–XTi solder alloys was examined by optical microscopy (OM, AXIO Scope A1, ZEISS) and scanning electron microscopy (SEM, S-3000H, Hitachi Co.). All specimens were ground with sandpaper, polished with 1 lm, 0.3 lm and 0.05 lm Al_2O_3 powders, and etched with 5% HCl and 95% H_2O solution. X-ray diffraction (XRD, D/max 2500V/PC) was used to determine phase composition.

2.4. Mechanical property

Hardness tests were carried out on a Vickers scale using an automatic digital microhardness tester (Highwood Model HWDM-3, TTS Unlimited Inc., Osaka). A dwell time of 10 s was used for loading of 0.1 N during measurement of the microhardness of the samples. The experiments were carried out at a room temperature of 25 °C. Tensile tests (MTS Tytron 250) were performed on specimens with a dog-bone shape and a gage section of $2 \times 3 \times 8$ mm³ at a constant strain rate of 1×10^{-2} s^{-1} at room temperature.

3. Results and discussion

3.1. Differential scanning calorimetry

Fig. 1 shows the DSC curves of lead-free SAC–XTi solder specimens doped with different concentrations of active Ti elements. The solidus temperature (T_s), liquidus temperature (T_L) and melting range ($\Delta T = T_L - T_S$) of these alloys were calculated
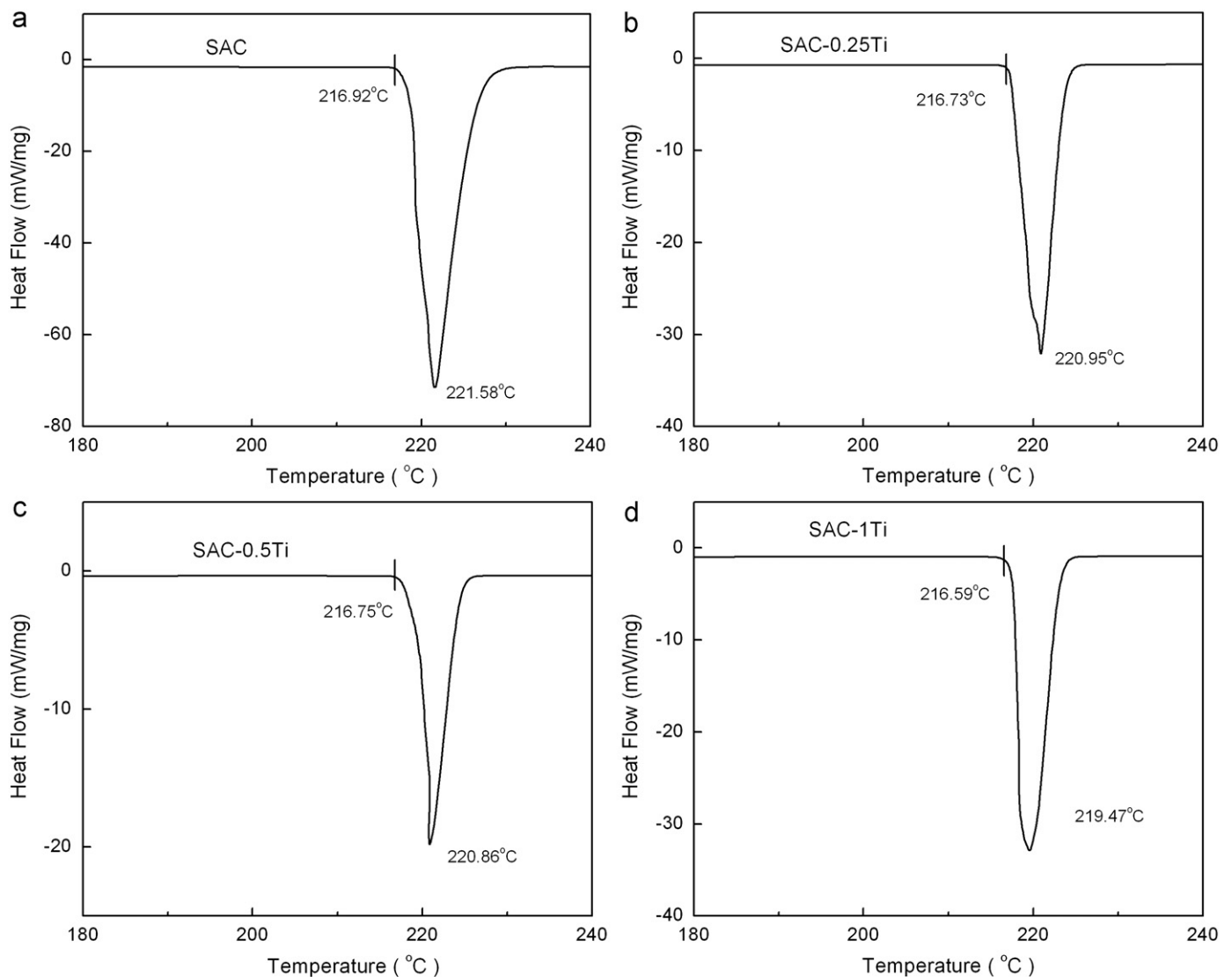

Fig. 1. DSC curves of the lead-free SAC–XTi solders: (a) SAC, (b) SAC–0.25Ti, (c) SAC–0.5Ti, and (d) SAC–1Ti.

and presented in Table 1. Fig. 1a exhibits the DSC curve of the lead-free SAC solder without any addition. Fig. 1b–d shows the DSC scans of lead-free SAC solders reinforced with 0.25 wt%, 0.5 wt%, and 1 wt% of active Ti, respectively. During the heating process of the DSC analysis, only one eutectic peak is observed in the lead-free SAC solder (Fig.1a). As shown in Fig.1 and Table 1, the liquidus temperatures were 220.95, 220.86 and 219.47 °C for SAC–0.25Ti, SAC–0.5Ti and SAC–1Ti, respectively, as compared with 221.58 °C for SAC solder. With increase in the addition of Ti, the liquidus temperatures decreased only slightly (about 0.63–2.11 °C). Another, it was found that the melting range (ΔT) decreased with increases in the addition of Ti (from 4.66 to 2.88 °C), indicating that adding the Ti moved the near-eutectic SAC alloy composition close to the eutectic value. In especially, the melting range of SAC–1Ti solder is very narrow, that is, is less than 4 °C. It is indicated that SAC–1Ti solders have excellent thermal properties, because the narrow melting range shows that alloys exist as part liquid for a short time during solidification and can form reliable joints in the reflowing process. This is consistent with previous conclusions [20,21].

Many studies have revealed that additions of transition metals (TM) and rare earths (RE) to Sn–Ag–Cu alloy provide marked improvements in melting characterization properties [22–29]. Chen et al. [26] confirmed that Ti addition being very effective in reducing the undercooling in the Sn-rich solders. Lin et al. [27]

worthy of notice reported that the degree of undercooling for proeutectic Sn was strongly affected by addition of trace transition metals (Mn and Ti) into SAC solders. The SAC105–0.5Ti sample exhibited an extremely suppressed undercooling of only 4 °C. A similar phenomenon was observed in Sn3.5Ag–XCo solder [28]. The amounts of undercooling of normal Sn3.5Ag and the Co-mixed Sn3.5Ag solder were 29.1 and 3 °C, respectively. The presence of Co particles in molten Sn3.5Ag solder provides nucleation sites for solidification. Thus, the undercooling of the Co-mixed Sn3.5Ag solder could be reduced. Cho et al. [29] reported that alloying elements with a hexagonal closed packed (HCP) structure may enhance the heterogeneous nucleation of β-Sn and thereby reducing its undercooling. This suggests that a small amount of Ti addition to SAC solder will significantly change their microstructure and reducing its undercooling.

3.2. Microstructure

Optical micrographs of as-solidified SAC, SAC–0.25Ti, SAC–0.5Ti, and SAC–1Ti solders are shown in Fig. 2. In order to precisely determine the influence of alloy elements Ti on the morphology of grain size, we analyzed the sizes of the β-Sn grains and the width of the eutectic area in 25 randomly chosen locations of the fabricated solder specimens. The average values of these data are listed in Table 3. The microstructures of SAC alloys have apparently both light regions of coarse β-Sn grains with an average size of 24.8 ± 5.9 μm and dark eutectic regions consist of mainly Ag₃Sn IMC and β-Sn matrix, as shown in Fig. 2a. The width of the eutectic area is about 6.8 ± 2.8 μm. With the addition of Ti, the solidified microstructure exhibits both more uniform microstructure and huge narrowing of eutectic bands, as shown in Fig. 2c and d.

SEM micrographs present the details of the configuration of SAC–XTi solders. Fig. 3 shows the microstructures of SAC solder alloys with different Ti contents. Typically, a coarse of dendritic β-Sn grains and thicker of eutectic areas (β-Sn+Ag₃Sn) were

Table 1
Solidus, liquidus, and melting range of the lead-free SAC–XTi in this study.

Specimens	Ti (wt%)	T_S (°C)	T_L (°C)	ΔT (°C)
SAC	Nil	216.92	221.58	4.66
SAC–0.25Ti	0.25	216.73	220.95	4.22
SAC–0.5Ti	0.5	216.75	220.86	4.11
SAC–1Ti	1	216.59	219.47	2.88

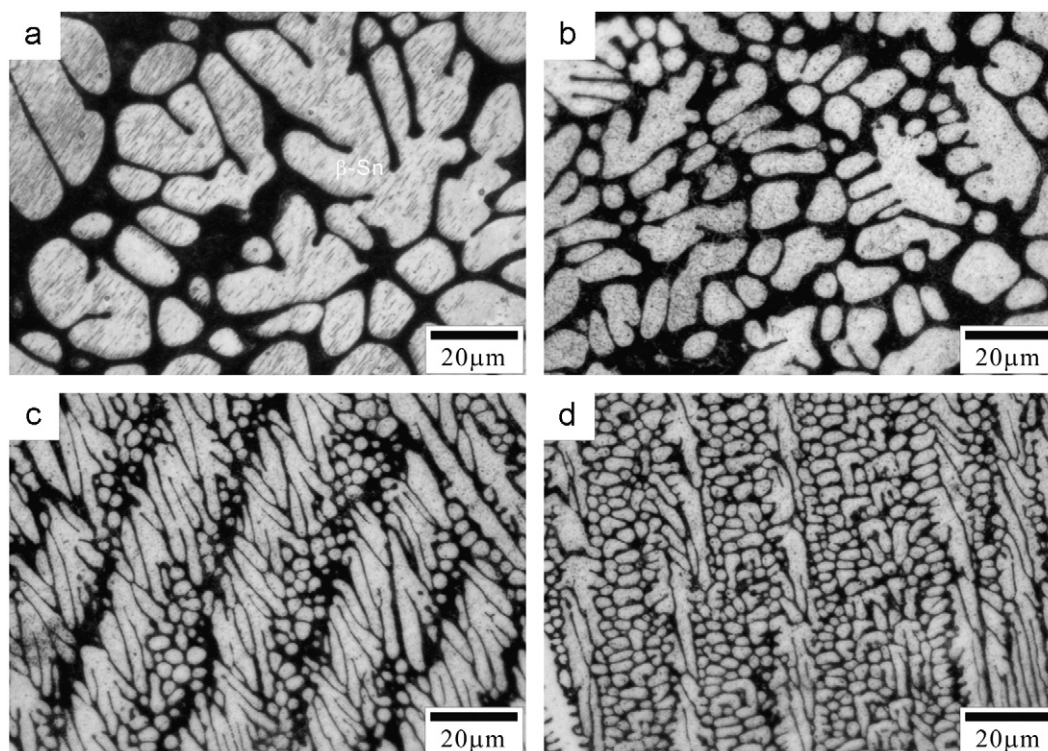T_S: solidus; T_L: liquidus; and ΔT: melting range.

Fig. 2. Micrographs showing the microstructures of as solidified lead-free SAC–XTi solders: (a) SAC, (b) SAC–0.25Ti, (c) SAC–0.5Ti, and (d) SAC–1Ti.

found in the SAC solder (Fig.3a). With the addition of Ti, the grain size of β-Sn and width of the eutectic area become very fine, as shown in Fig. 3c and d. When 1 wt% was added (Table 3), the grain size of β-Sn was about 4.8 ± 1.7 μm (vs. 24.8 ± 5.9 μm of SAC), and the width of the eutectic area was 1.2 ± 0.4 μm (vs. 6.8 ± 2.8 μm of SAC). The reason is due to the unique properties of active Ti elements. Alloying element of Ti gave rise to the appearance of heterogeneous IMC and a morphological change of eutectic IMC, as well as a higher area fraction of primary β-Sn but a reduced dendritic size. Those effects were intensified with a greater amount of additives. Generally, grain refinement can be understood to be directly related to the nucleation and growth process of Sn grains. This is based on the nucleation ideas of the Volmer and Weber model [30,31]. According to heterogeneous nucleation theory, the equation can be written as follows:

$$\text{Driving force for solidification}: \quad \Delta G_v \cong \Delta T \Delta S = \frac{\Delta H_f \Delta T}{T_m} \qquad (1)$$

$$\text{Critical nucleus size}: \quad \gamma^* = \frac{-2\gamma_{sL}}{\Delta G_v} \qquad (2)$$

$$\text{Free energy barrier}: \quad \Delta G^* = \frac{16\pi\gamma_{sL}^3}{3\Delta G_v^2} f(\theta) \qquad (3)$$

where ΔT is the undercooling below the liquidus temperature K, ΔS the entropy change for liquid to solid phase transformation, J/K/m³, ΔH_f the enthalpy of solidification, T_m the melting temperature, $f(\theta)$ is a function of the contact angle (θ), γ_{sL} is the interface surface energy of a solid–liquid interface in J/m², G_v is the driving force for solidification. Fig. 4 shows the solid nucleating on a substrate in a liquid [31]. Therefore, it can be seen that if contact angle (θ) is close to zero, wetting of the heterogeneous substrate for nucleation is promoted and nucleation rate increases. The standard Gibbs free energy of formation for Ti–Sn IMC is also lower than that for Ag–Sn, Cu–Sn, Ti–Cu, and Ti–Ag in both Ag–Sn–Ti and Cu–Sn–Ti systems [26,32,33], Therefore, the addition of trace Ti to the SnAgCu solder

forms fine Ti–Sn precipitates. Some research work has revealed this phenomenon [13,25–29,34–36]. With the addition of Ti (Fig. 3b), some massive IMC particles, named heterogeneous IMC, were found, rather than Ag₃Sn. According to Energy Dispersive Spectroscopy (EDS) analysis, as shown in Fig. 5, the chemical composition (wt%) of the heterogeneous IMC (darker) contained Sn (83.98.%),
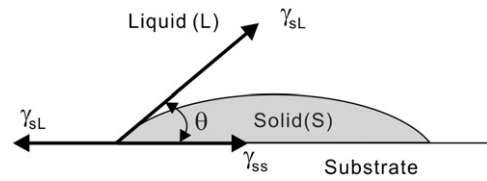

Fig. 4. Schematic representation showing the formation of spherical cap of solid (s) on a substrate, contact angle and surface tension forces [31].
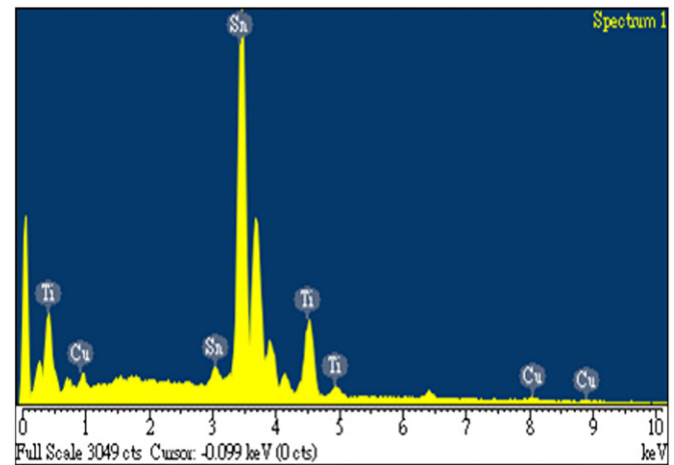

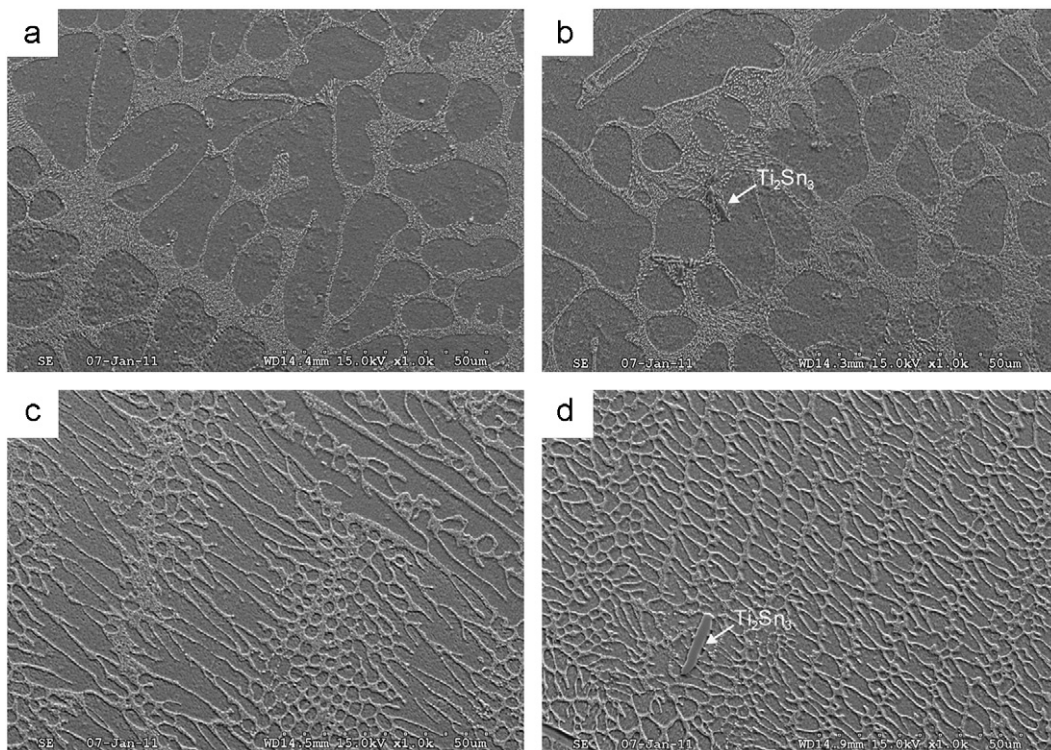**Fig. 5.** EDS analysis results of the dark IMC in Fig. 3d.

Fig. 3. SEM photographs of the lead-free SAC–XTi solders: (a) SAC, (b) SAC–0.25Ti, (c) SAC–0.5Ti, and (d) SAC–1Ti.
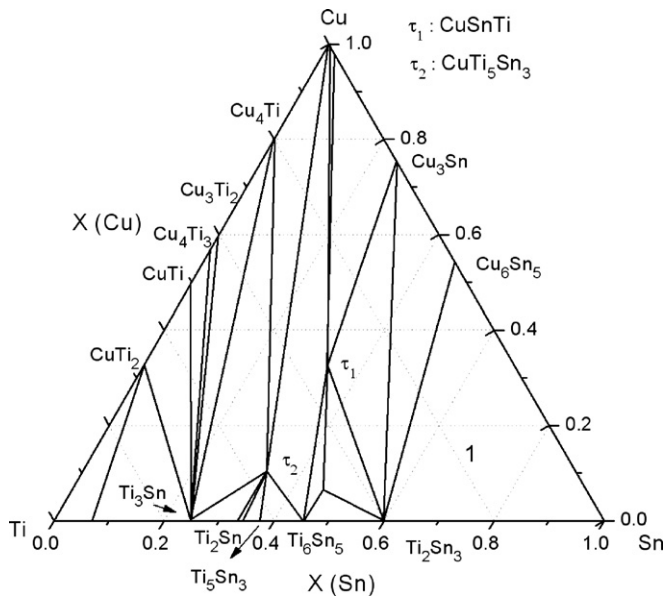
Fig. 6. Calculated isothermal section at 150 °C from the Sn–Cu–Ti ternary system [40].
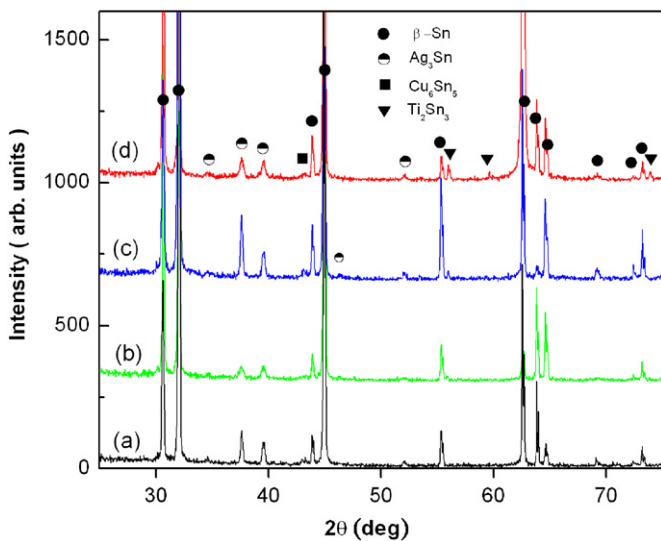

Fig. 7. XRD analysis of the lead-free SAC–XTi solders: (a) SAC, (b) SAC–0.25Ti, (c) SAC–0.5Ti, and (d) SAC–1Ti.

Cu (3.82%), and Ti (12.20%). Therefore, it is suggested that the ternary compound Ti–Sn–Cu or mixing of Ti–Sn, Cu–Sn, and Sn exists in the present heterogeneous IMC. However, two ternary compounds (i.e., $CuTi_5Sn_3$ and CuTiSn) and their crystal structural data have been reported [37,38]. No new ternary compound was found. From Fig. 6 [39], one can see that local equilibrium (Mark 1) is fulfilled in this structure, as Ti_2Sn_3, Cu_6Sn_5 and Sn can all exist in equilibrium. It has been confirmed that the binary compound Ti_2Sn_3 exists in the SAC–XTi solder alloy. Lin et al. [27] investigated the effects of Ti additives on the microstructure and solidification behavior of Sn1.0Ag0.5Cu (SAC105) alloys. Ti_2Sn_3 IMC was observed in Ti-doped SAC105 samples. Chen et al. [26] found that small Ti alloying additions to Sn–Ag and Sn–Cu solders produced a similar phenomenon. According to the Ti–Sn binary system [40], the heterogeneous Ti–Sn IMC can be Ti_2Sn_3 phases.

Fig. 7 shows X-ray diffraction patterns of the SAC–XTi solders. Fig. 7a shows the XRD spectrum of the SAC solder without any Ti added. The patterns of SAC solder show diffraction peaks for β-Sn,

Ag_3Sn, and Cu_6Sn_5. Fig. 7b–d shows the X-ray diffraction patterns of SAC solder doped with Ti. As the percentage of Ti increases in the solder matrix, the intensity of the peak observed at a 2θ angle of 56.03° becomes stronger, demonstrating the presence of Ti_2Sn_3 IMC in the SAC–XTi solder specimen. From these results, we anticipated that the microstructural change would affect the mechanical properties of the solder alloy.

Table 2
Microhardness measurements of the SAC–XTi solders.

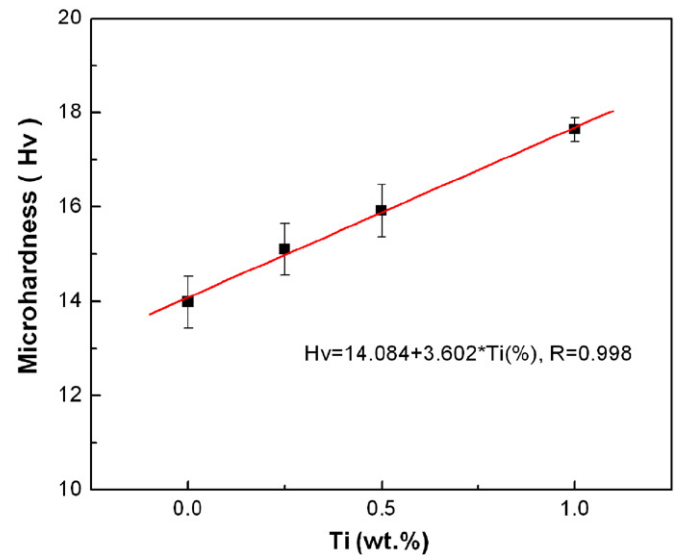| Sample #	Addition (wt%)	Microhardness indention results (H_v)					
		Trial 1	Trial 2	Trial 3	Trial 4	Trial 5	Average
SAC	Nil	13.4	14.5	13.4	14.5	14.1	13.98
1	0.25	15.9	14.9	15.8	14.8	14.9	15.10
2	0.5	16.4	15.3	16.2	15.8	15.9	15.92
3	1	17.9	17.4	17.9	17.4	17.6	17.64

Fig. 8. Effect of Ti addition on the microhardness of the SAC–XTi solders.
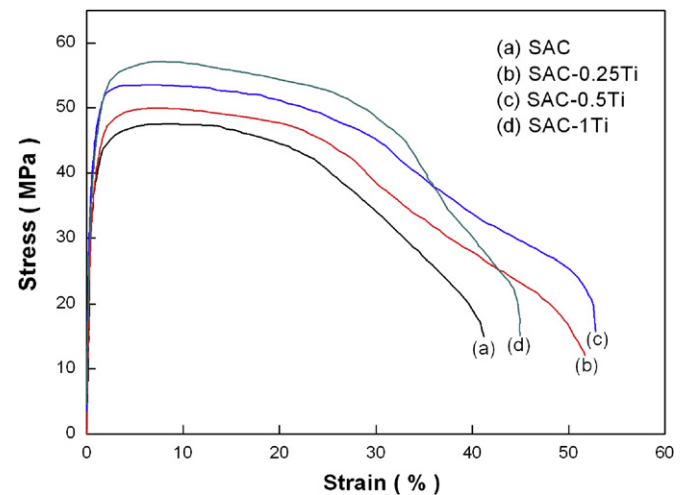

Fig. 9. Engineering stress–strain curves of the SAC–XTi solders: (a) SAC, (b) SAC–0.25Ti, (c) SAC–0.5Ti, and (d) SAC–1Ti.

3.3. Mechanical property

The differences in microstructure of the SAC–XTi alloys, especially the change in size of β-Sn grains, results in changes to the mechanical properties. The influence of Ti reinforcement on the microhardness of the SAC–XTi solders is summarized in Table 2. The microhardness enhancement of these solders was 8.0–26.1% over that of the SAC solder. A plot of the microhardness (H_v) versus Ti content is shown in Fig. 8. Linear regression analysis of the experimental data yielded:

$$H_v = 14.084 + 3.602Ti(wt\%) \tag{4}$$

Fig. 9 shows the typical tensile stress–strain curves of the SAC–XTi solder specimens at a constant strain rate of $1 \times 10^{-2}\,s^{-1}$ at room temperature. The analysis tests were conducted on three different samples taken from the same specimen, and the average values of the ultimate tensile strength (UTS), 0.2% yield strength (0.2YS), and percentage of elongation are given in Table 3. The UTS, 0.2YS, and elongation values of SAC solder were 47.2 ± 4.8 MPa, 42.1 ± 3.6 MPa, and $41.1 \pm 5.2\%$, respectively. The UTS and 0.2YS of SAC–XTi solders increased with increased Ti content, both dramatically and linearly. Another, the total elongation increase of the lead-free SAC–1Ti solder was slight high than that of the lead-free SAC solder (44.9 ± 4.8 vs. $41.1 \pm 5.2\%$). For example, with the addition of 1 wt% Ti, the UTS and 0.2YS rose to 57.6 ± 3.8 and 54.5 ± 4.7 MPa,

respectively. Another, the total elongation was improved by 0.25–0.5 wt% addition of Ti alloying elements into the SAC solder. However, when the Ti concentration up to over 1.0 wt% decreased the beneficial influence. The presence of the large Ti_2Sn_3 IMC precipitates (Fig.3d) in the SAC–1Ti solder is clearly seen to affect elongation. Fig. 10 shows the fracture surfaces of the tensile specimens of SAC–XTi solders tested at room temperature (25 °C) and strain rates of $1 \times 10^{-2}\,s^{-1}$. The fracture surface of SAC–XTi alloys displays ductile dimples, that are oriented in the loading direction. It can be seen in Fig.10a that the fracture surface of SAC specimens had many coarse dimple. A comparison of Fig. 10a with Fig. 10b–d indicates that adding Ti to the SAC alloy refines the dimples size. In summary, the microstructure of SAC–XTi solder was stabilized and refined by the alloying elements, exhibiting mechanical properties superior to those of SAC solder alloys.

Generally, metals and alloys having a finer grain structure possess a higher 0.2YS and/or higher microhardness, owing to the Hall–Petch relationship. According to the Hall–Petch equation, the relationship between solder alloy 0.2YS (σ_y) and mean grain size (d) can be written as follows [41]:

$$\sigma_y = \sigma_o + K.d^{-1/2} \tag{5}$$

where σ_o and K are material constants. Fig. 11 presents the linear regression analysis of the experimental data, the dependence of 0.2YS on the reciprocal square root of d for the SAC–XTiO$_2$

Table 3
Tensile tests for the lead-free SAC–XTi older.

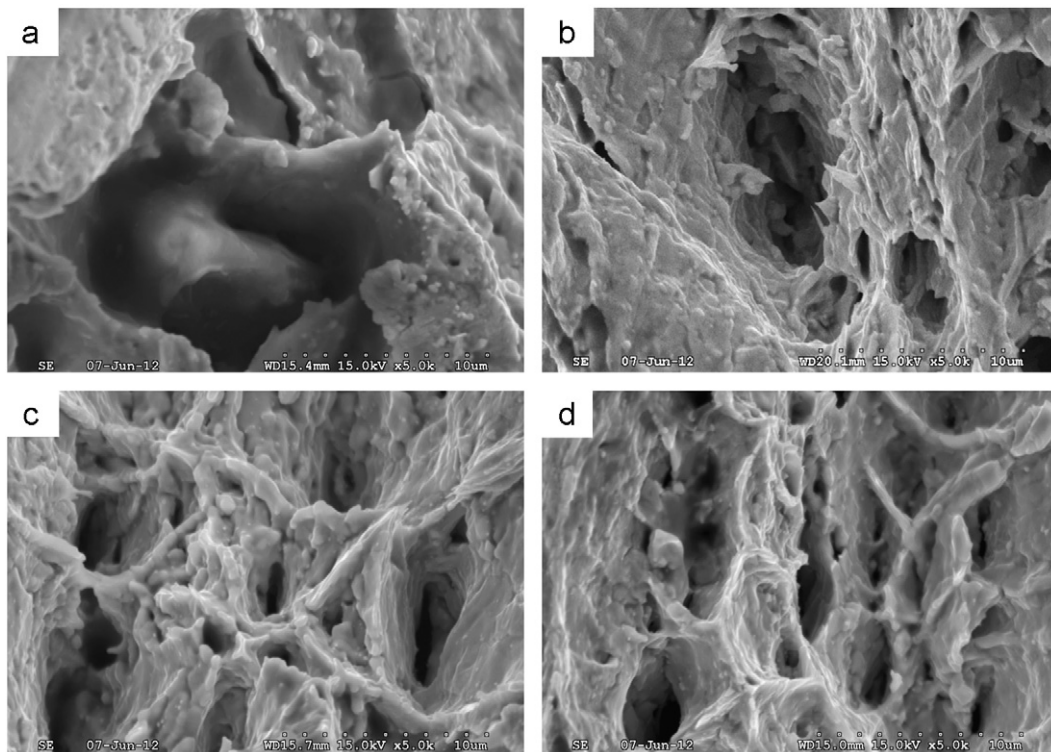| Specimens	Ti (wt%)	β-Sn (μm)	Width of eutectic area (μm)	UTS (MPa)	0.2YS (MPa)	Elongation (%)
SAC	Nil	24.8 ± 5.9	6.8 ± 2.8	47.2 ± 4.8	43.1 ± 3.6	41.1 ± 5.2
SAC–0.25Ti	0.25	13.2 ± 4.2	4.5 ± 1.2	50.1 ± 4.6	46.3 ± 4.2	51.2 ± 4.6
SAC–0.5Ti	0.5	7.2 ± 2.1	2.1 ± 0.8	53.2 ± 5.2	52.1 ± 4.5	52.6 ± 3.4
SAC–1Ti	1	4.8 ± 1.7	1.2 ± 0.4	57.6 ± 3.8	54.5 ± 4.7	44.9 ± 4.8

Fig.10. SEM showing the tensile fracture surfaces of solder s subjected to uni-axial tensile deformation at room temperature (25 °C) and strain rates of $1 \times 10^{-2}10^{-2}\,s^{--1}$: (a) SAC, (b) SAC–0.25Ti, (c) SAC–0.5 Ti, and (d) SAC–1Ti.
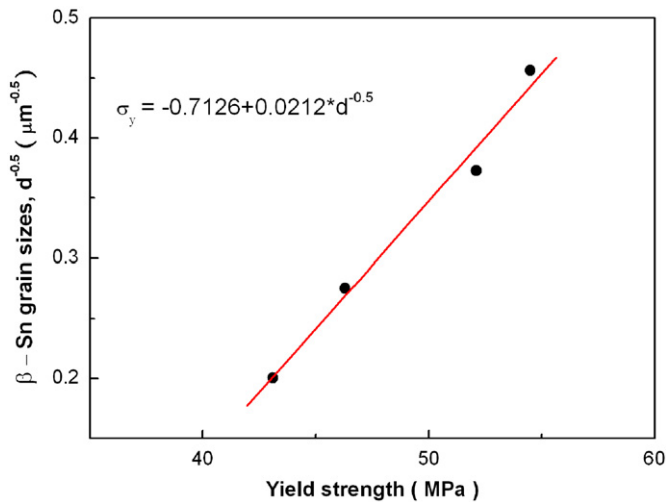
Fig. 11. The 0.2YS (σ_y) of the SAC–XTi solders plotted vs. the inverse-square root of β-Sn grain size d.

composite solders ($X=0$–1.0 wt%). Linear regression analysis of the experimental data yielded an equation for the 0.2YS of the specimens:

$$\sigma_y = -0.7126 + 0.0212 \times d^{-1/2} \tag{6}$$

Most of the linear correlation coefficient values (R^2) for these plots were greater than 0.99. This equation indicates a relationship such that the finer the β-Sn grain, the larger the increase in alloy strength. From the tensile data and the microstructure information, it can be concluded that the addition of Ti can significantly strengthen Sn3Ag0.5Cu. Such a strengthening effect can be attributed to the refined β-Sn, Ag_3Sn, and T_2Sn_3 IMCs as a result of adding a fourth element. Such degradation in ductility is attributed to the formation of large precipitates (Fig.3d).

4. Conclusions

In the present work, the effects of Ti element additions to SAC solder alloys on the thermal analysis, microstructural and mechanical properties were examined. The results are summarized as follows:

(a) The melting temperatures of the SAC–XTi ($X=0.25$–1 wt%) solders are only slightly lower than that of the SAC solder, by about 0.63–2.11 °C. At the same time, the melting range temperature ($\Delta T = T_L - T_S$) decreases with increases in the addition of Ti.
(b) With the addition of trace Ti, the coarse β-Sn grains in Sn3.5Ag0.5Cu alloy become finer and uniform, the eutectic colony becomes narrower, and the new Ti_2Sn_3 IMC develop.
(c) The UTS, 0.2YS, and microhardness of the SAC–XTi solder increase with increases in alloying Ti content of 0.25–1.0 wt%. However, when the Ti concentration exceeds 1.0 wt%, the elongation is decreased.

References

[1] K.N. Tu, K. Zeng, Mater. Sci. Eng. R34 (2001) 1–58.
[2] J.C. Leong, L.C. Tsao, C.J. Fang, C.P. Chu, J. Mater. Sci. Mater. Electron. 22 (2011) 1443–1449.
[3] T.H. Chuang, S.F. Yen, M.D. Cheng, J. Electron. Mater. 35 (2006) 302–309.
[4] K.S. Kim, J. Alloys Compd. 352 (2003) 226–236.
[5] R.W. Wu, L.C. Tsao, S.Y. Chang, C.C. Jain, R.S. Chen, J. Mater. Sci. Mater. Electron. 22 (2011) 1181–1187.
[6] L.L. Gao, S.B.L. Zhang, Z. Sheng, F. Ji, W. Dai, S.L. Yu, G. Zeng, Microelectron. Eng. 87 (2010) 2025–2034.
[7] L.C. Tsao, S.Y. Chang, Mater. Des. 31 (2010) 990–993.
[8] L.C. Tsao, Mater. Sci. Eng. A 529 (2011) 41–48.
[9] L.C. Tsao, S.Y. Chang, C.I. Lee, W.H. Sun, C.H. Huang, Mater. Des. 31 (2010) 4831–4835.
[10] T.H. Chuang, M.W. Wu, S.Y. Chang, S.F. Ping, L.C. Tsao, J. Mater. Sci. Mater. Electron. 22 (2011) 1021–1027.
[11] P. Liu, P. Yao, J. Liu, J. Electron. Mater. 37 (2008) 874–879.
[12] A.K. Gaina, T. Fouzdera, Y.C. Chana, W.K.C. Yung, J. Alloys Compd. 509 (2011) 3319–3325.
[13] D.Q. Yu, J. Zhao, L. Wang, J. Alloys Compd. (2004) 170–175.
[14] C.M.L. Wu, D.Q. Yu, C.M.T. Law, L. Wang, Mater. Sci. Eng. R 44 (2004) 1–44.
[15] M. Humphries, Congressional Research Service Technical Report R41347, 2011.
[16] K.R. Cardoso, D.N. Travessa, A.G. Escorial, M. Lieblich, Mater. Res. 10 (2007) 199–203.
[17] S.Y. Chang, T.H. Chuang, L.C. Tsao, C.L. Yang, Z.S. Yang, J. Mater. Process. Technol. 202 (2008) 22–26.
[18] W.P. Liu, P. Bachorik, N.C. Lee, Proceedings of the 58th Electronic Components and Technology Conference, ECTC, 2008, pp. 452–458.
[19] W.P. Liu, N.C. Lee, J. Mater. 59 (2007) 26–31.
[20] H. Hao, J. Tian, Y.W. Shi, Y.P. Lei, Z.D. Xia, J. Electron. Mater. 36 (2007) 766–774.
[21] J. Zhou, Y. Sun, F. Xue, J. Alloys Compd. 397 (2005) 260–264.
[22] L. Zhang, C.W. He, Y.H. Guo, J.G. Han, Y.W. Zhang, X.Y. Wang, Microelectron. Reliab. 52 (2012) 559–578.
[23] H. Mavoori, A.G. Ramirez, S. Jin, Appl. Phys. Lett. 78 (2001) 2976–2978.
[24] T.H. Chuang, H.F. Wu, J. Electron. Mater. 40 (2011) 71–77.
[25] L.C. Tsao, C.H. Huang, C.H. Chung, R.S. Chen, Mater. Sci. Eng. A 545 (2012) 194–200.
[26] W.M. Chen, S.K. Kang, C.R. Kao, J. Alloys Compd. 520 (2012) 244–249.
[27] L.W. Lin, J.M. Song, Y.S. Lai, Y.T. Chiu, N.C. Lee, J.Y. Uan, Microelectron. Reliab. 49 (2009) 235–241.
[28] J.S. Lee, K.M. Chu, R. Patzelt, D. Manessis, A. Ostmann, D.Y. Jeon., Microelectron. Reliab. 85 (2008) 1577–1583.
[29] M.G. Cho, H.Y. Kim, S.K. Seo, H.M. Lee, Appl. Phys. Lett. 95 (2009) 021905.
[30] D.A. Porter, K.E. Easterling, Phase Transformations in Metals and Alloys, , 1992. (pp. 185–207).
[31] K.T. Kashyap, T. Chandrashekar, Bull. Mater. Sci. 24 (2001) 345–353.
[32] J. Wang, C. Liu, C. Leinenbach, U.E. Klotz, P.J. Uggowitzer, J.F. Loffler, Calphad Comput. Coupling Phase Diagrams Thermochem. 35 (2011) 82–94.
[33] X. Zhang, Y. Zhan, Q. Guo, G. Zhang, J. Hu, J. Alloys Compd. 480 (2009) 382–385.
[34] H. Hao, J. Tian, J. Electron. Mater. 36 (2007) 766–774.
[35] Y. Yu, Z.D. Xia, F. Guo, Y.W. Shi, J. Electron. Mater. 37 (2008) 975–981.
[36] K.S. Kim, S.H. Huh, K. Suganuma, Microelectron. Reliab. 43 (2003) 259–267.
[37] N.O. Koblyuk, L.G. Akselrud, R.V. Skolozdra, Pol. J. Chem. 73 (1999) 1465–1471.
[38] S. Hamar-Thibault, C.H. Allibert, J. Alloys Compd. 317–318 (2001) 363–366.
[39] V. Vuorinen, H.Q. Dong, T. Laurila, J. Mater. Sci. Mater. Electron. 23 (2012) 68–74.
[40] T.B. Massalski, Binary Alloy Phase Diagram, 2nd ed., ASM International, Metals Park Press, Ohio, 1990.
[41] T.H. Chuang, L.C. Tsao, C.H. Chung, S.Y. Chang, Mater. Des. 39 (2012) 475–483.